Proceedings of the 12th World Congress on Electrical Engineering and Computer Systems and Sciences (EECSS'25)
Paris, France – August 17 - 19, 2025
Paper No. ICBES 135
DOI: 10.11159/icbes25.135

Using Robotic Laser Ablation System to Study Cellular Stress Responses

David Z. He[1,†], Sophia Liu[1,†], Veronica Gomez-Godinez[1], Zachary Wang[1], Chengbiao Wu [2], Linda Shi[1*]
[1]Institute of Engineering in Medicine, University of California Sand Diego, La Jolla, California, USA
[2]Department of Neurosciences, University of California San Diego, La Jolla, CA 92093, USA
***** Correspondence: zshi@ucsd.edu
†High school students participating in IEM OPALS program, equally contributed

Abstract **-** Laser ablation is an established process for analyzing cellular responses to damage. By utilizing the specificity and visualization capabilities of a femtosecond laser in conjunction with fluorescent dyes and image analysis applications, this contemporary laser ablation methodology is a promising process for emulating and analyzing cellular reactions affected by degenerative diseases and other diseases characterized by cellular stress responses. In this study, we evaluated the methodology using two cell types: primary mouse cortical neurons and myocardial cells. We used Quantitative Phase Imaging to analyze the changes in the thickness of PC12 cells, HEK293 cells, and collagen tissue. In mouse primary cortical neurons, laser ablation was applied to assess axonal responses under varying glucose concentrations. In myocardial cells, laser ablation was used alongside nucleic acid dyes to evaluate cellular reactions to neighboring cell death. Although definitive results have yet to be reached, the laser ablation model is thus a viable approach for simulating and analyzing cellular degeneration.

Keywords: Laser Ablation; Cellular Degeneration; Heart Cell; Cortical Neuron; Quantitative Phase Imaging

1. Introduction

Laser ablation, a cutting-edge technique in the realm of cellular research, has emerged as a powerful tool with profound implications for understanding the intricacies of cellular degeneration and damage. Its versatility has been demonstrated across various research domains, including investigating DNA repair in cancer cells, studying neuronal responses to shear forces, and establishing models of traμmatic brain injury, among others [1]. However, this study proposes that laser ablation can be used in a variety of other fields, namely in the study of cellular degeneration. Through the application of laser ablation on different types of tissues, we gain the opportunity to explore the mechanisms that govern cellular behavior in the face of pathological changes, enabling us to uncover insights that may ultimately lead to the development of targeted interventions or therapies. In this study, we used laser ablation to uncover the pathophysiological processes underlying PC12, HEK293, and collagen through Quantitative Phase Imaging (QPI) and two types of cellular degeneration: Cortical neuron degeneration from diabetes and heart cell degeneration in cardiomyocytes. Our research aims not only to contribute fresh insights but also to underscore the efficacy of laser ablation as a potent tool for investigating similar degenerative diseases. This research study seeks to implement laser ablation in a variety of fields, replicating and analyzing the effect of cellular stressors on degenerative diseases. The precision provided by the robotic laser microscope (RoboLase) system allows for more exact replication and versatility of experiments, and through a combination of fluorescent dyes and image analysis tools such as MATLAB or ImageJ, can accurately quantify and compare cellular responses to damage.

Diabetic peripheral neuropathy (DPN), a severe complication of diabetes, results from high glucose-induced nerve damage [2], causing pain, numbness, and weakness. Using the RoboLase system, we investigated how glucose levels affect the processes of cortical neuron resistance to damage. Similarly, myocardial infarction (MI) leads to tissue hypoxia and cell death [3]. Our study explored the ischemic border zone in mouse cardiomyocytes, focusing on cellular responses and the "loss of neighbor" hypothesis [4]. By analyzing changes and factors like oxygen gradients, we aim to uncover mechanisms of DPN and MI and identify therapeutic targets.

Quantitative Phase Imaging (QPI) is an emerging technique that offers a label-free, non-destructive method to measure cellular and tissue properties. In another context, a metasurface is an engineered two-dimensional structure composed of subwavelength elements that manipulate light at the nanoscale, enabling precise control of phase, amplitude, and polarization [5-8]. Therefore, the metasurface-based approach enhances the QPI system by making it more stable, reliable, and compact

[9-11]. By quantifying phase shifts in light passing through a sample, QPI enables the visualization and analysis of subtle changes in refractive index, often indicative of alterations in cellular structure and function [12].

This study demonstrates two QPI applications: monitoring live cell thickness after laser ablation in PC12 and HEK293 cell lines and measuring collagenous tissue thickness post-ablation. Laser-induced cellular manipulation is pivotal in biomedical research, enabling precise studies on laser parameters like power to optimize techniques and reduce damage. QPI provides a robust tool to assess laser-induced changes in cellular structures and collagen fibers, which is vital for understanding diseases like scleroderma and systemic sclerosis. These findings highlight QPI's potential for advancing therapeutic strategies and exploring new applications in biomedical research.

2. Materials and Methods

2.1. RoboLase Set Up

RoboLase, a robotic laser microscope system, utilized a Mai Tai femtosecond laser to carefully ablate cells. The near-infrared laser scissors could be modulated easily in both terms of intensity and spatiotemporal position, allowing surrounding regions to remain untouched. This system interfaced with a Zeiss inverted microscope through a series of reflective coated mirrors, which applies high numerical aperture objectives and light sensitive cameras for high resolution and sensitivity enhancement. Operating at a wavelength of 790 nm, with a pulse energy of 4 nJ and a changeable power depending on the experiment, the laser was directed through a 40x objective lens to precisely target the intended cells. The ablation process followed meticulously drawn lines, and the QuantEM camera captured detailed images throughout the procedure. [12]

2.2. Axonal Strength (Glucose Study)

Cortical neurons were collected from the cerebral cortex of P0 mouse pups cultured in Neurobasal A (GIBCO #11090-081) supplemented with 5% FBS Glutmax and B-27 supplements [13]. Cortical neurons were then treated with maintenance media (Neurobasal A, Glutmax, B27) containing either normal (3 mM) or high (25 mM) levels of glucose. After being cultured at these different glucose levels for about 40 minutes, the axons were damaged 20 microns away from the cell body, using the femtosecond laser at a power of 225-275 mw before the 40x objective.

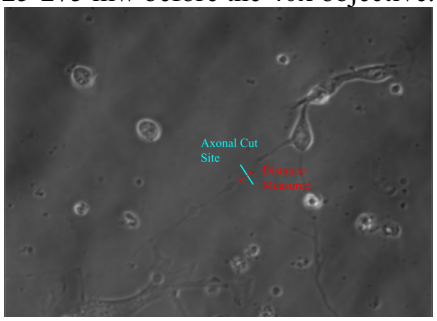

Figure 1. A sample cortical neuron with an axonal cut site (blue). Axonal strength is measured by the axonal gap (red)

Phase images before and after the laser were collected at 5-minute intervals. Images were analyzed in ImageJ– the shrinkage created due to laser-inflicted damage was recorded in pixels. The data of interest (pre-cut, post 30 seconds, post 5 minutes, post 10 minutes, and post 15 minutes) were collected and grouped based on the mediμm the cells were cultured in (high glucose media and normal glucose media). The average length of the shrinkage was then calculated based on the post time and graphed accordingly.

2.3. Cardiomyocyte Study

The neonatal rat cardiomyocytes were isolated from hearts using the Worthington Neonatal Cardiomyocyte Isolation System [14]. The hearts were chilled and rinsed with CMF-HBSS and then refrigerated in 50 μg/mL Trypsin. Twenty-four hours later, the tissue was warmed, oxygenated, and transferred into collagenase. Tubes were triturated to release cells and suspended and sedimented in Leibovitz L-15. Following a 4-day culture with a 2μg/cm^2 fibronectin, the cells were stained with SYTOXTM Orange Nucleic Acid Stain twenty minutes before ablation.

Laser ablation patterns were drawn by hand using specialized imaging software, which when initiated, guides the laser through the triangular pattern drawn to ablate the cells. An example of this can be seen in the figure below. Laser ablation can replicate myocardial cell loss, creating an artificial border zone, which allows us to replicate the effects on border cells from the loss of neighboring cells. The TrackMate-StarDist extension on ImageJ was used to create masks and collect the normalized area of border cells at frames before and after ablation. The border cells are marked with red tracks in the phase image below. Through a MATLAB code, this data could then be assembled and graphed into several "tracks".

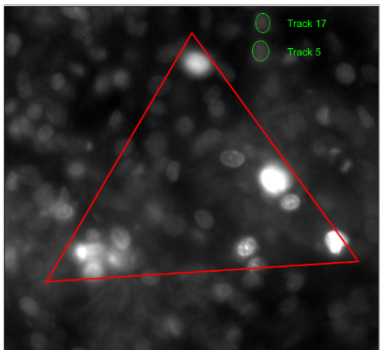

Figure 2. Phase image with indication of laser ablation area (triangle) and track indications (circles)

2.4. Quantitative Phase Imaging

For PC-12 cells, the cover glasses were pre-coated with 0.1% PDL before plating. Then, the PC-12 cells were plated using DMEM high glucose,1% penicillin/streptomycin, 10% horse serµm, and 5 % fetal bovine serµm. The cells were stored at 37°C 5% CO_2 incubator. The quantitative phase imaging (QPI) methodology, FOSSMM, achieved 3D QPI to measure the PC-12 thickness. HEK 293 cells are grown on 60mm Nunc cell culture dishes (ThermoFisher) and in growth mediµm with 10% FBS and 1×Glutamax (Gibco, ThermoFisher), maintained at 37 °C and 5% CO_2. 1-2 days before ablation, the cells were washed three times with Hanks Buffered Saline Solution (HBSS; ThermoFisher) devoid of calciµm then gently detached with 1 mL of 1×TryplE Express Enzyme (Gibco, ThermoFisher) for 5 min, longer if detachment is not observed. Upon detachment, TryplE is quenched by the addition of 4 mL of growth medium, and the cells are then seeded onto imaging dishes [10]. For the collagenous tissue, Insoluble type I bovine tendon collagen (Advanced BioMatrix #5162) is reconstituted with a semi-solution of 0.01M HCl solution [15], which are later manually stretched to isolate collagen fibers for ablation.

For all experiments, the RoboLase III system was used to image the cells in the XY plane. A Mai Tai femtosecond laser (set to the wavelength of 780 nm) is guided into a Zeiss inverted microscope via a sequence of highly reflective coated mirrors and the 40x LUCPLFLN Bright field air objective for precise laser ablation damage on the cells and tissues. The ablation is applied precisely along a drawn line, with images being continuously captured using a QuantEM camera. As the ablation process follows the ablation pattern, images are captured before and after cutting the samples using a polarized camera. Any measurements later made are created using ImageJ and changes in thickness are delineated using a MATLAB code.

The ablation was carried out in a defined area and the resulting changes in tissue thickness were captured using a QPI methodology named Fourier optical spin splitting microscopy (FOSSMM) [9]. FOSSMM consists of two lenses, a metasurface, and a polarized camera, allowing for underfocused and overfocused images. The meta-device is 50 µm away from the flat surface of the substrate [16,17]. Imaging the same path is repeated at different depths within the sample thickness by adjusting the position of the sample relative to the focusing arrangement along the beam propagation direction. Using the differences between the images, the QPI is acquired using the transport of intensity equation (TIE) algorithm, [18] enabling real-time monitoring cell property changes.

3. Results and Discussion

3.1. Axonal Strength (Glucose Study)

Both high glucose and normal glucose (3 mM) showed clear signs of axonal damage after ablation(Figure 3). However, normal glucose (3 mM) neurons exhibited comparatively lower shrinkage than neurons in standard high glucose medium.

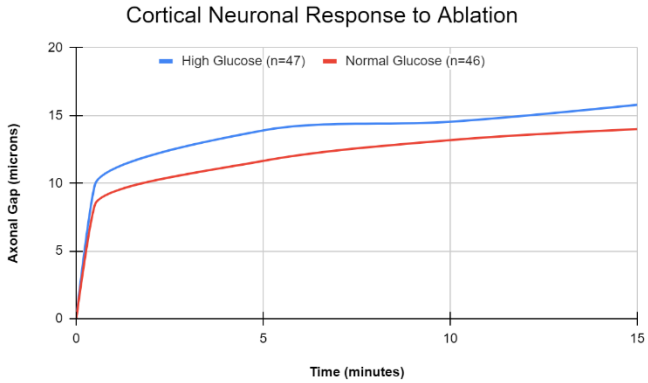

Figure 3. Graph of the axonal gap over time in response to ablation in cells with high glucose and normal glucose levels.

After initial ablation, neurons under high glucose exhibited an average of 9.9-micron shrinkage, while those under normal glucose (3 mM) exhibited an average shrinkage of 8.4 microns. Similarly, after fifteen minutes, neurons under high glucose exhibited a shrinkage of 15.8 microns, while the neurons under normal glucose (3 mM) exhibited a shrinkage of 14.0 microns. However, there was some significant variation observed in the data, with mean errors of 1.43 and 1.04 after fifteen minutes for high-glucose and low-glucose neurons respectively. Thus, with the number of trials obtained currently, we were unable to ascertain a significant change in shrinkage between the separate glucose conditions. Further research, trials, and data will need to be collected before these results can be ruled significant. However, these results still point to laser ablation as a viable method of testing axonal and neuronal strength due to extracellular conditions, such as the presence of glucose levels.

3.2. Cardiomyocyte Study

Multiple border cells outside the triangular ablation zone were chosen and tracked before and after ablation as shown in Figure 4. Their areas before ablation were normalized to have an area of 1. Many of these border cells experienced changes after the ablation, with three sample tracks being shown below. After ablation, the cell marked as “Track 5” increased by 10% in area and continued to increase in area before reaching a maximμm 20% increase. Similarly, tracks 17 and 19 demonstrated a 10% increase in area after ablation. Thus, by creating an artificial border zone with laser ablation, coupled image-tracking software can be used to ascertain changes in cellular shape, and thus the presence of irregular force and stress caused by the absence of neighboring cells. This opens many realms of possibilities when studying border zones caused by myocardial infarctions. For example, cells of different distances away from the border zone can be tracked separately to determine the effects of distance from the border zone on cellular stress.

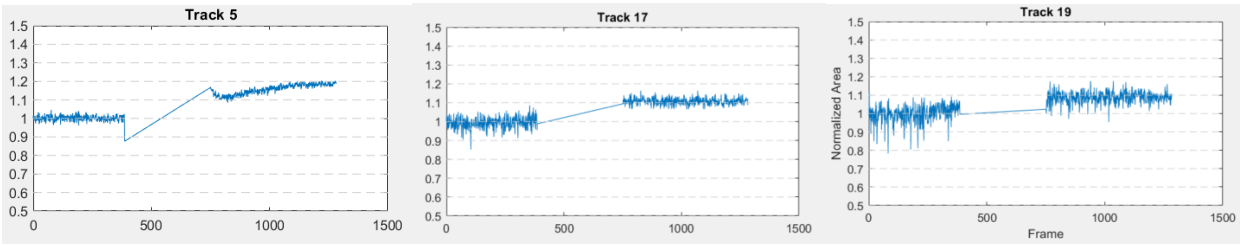

(a) (b) (c)

Figure 4. Measurements of normalized area of Heart Cells and the affected neighboring cells from various distances of the border zone. (a) Cellular Track 5 increases by 20% at the end of measurement. (b) Cellular Track 17 increases by 10% at the end of measurement. (c) Cellular Track 19 increases by 10% at the end of measurement.

The data proved that the loss of neighboring cells can indeed cause border cells to undergo changes. These irregular forces may play a large part in contributing to the growth of the border zone, as well as the development of cellular characteristics and niches specific to myocardial infarction cases. For future research, looking for patterns in the location of myocardial infarction relative to laser ablation by machine learning may make the spreading of border zones predictable. If the loss of neighboring cells is indeed due to mechanical stressors, the ability to predict which neighboring cells are susceptible to myocardial infarction expansion may allow for the development of treatments that stabilize heart tissue and neutralize mechanical stress before cell death by loss of neighboring cells occurs.

This laser ablation model also has a large potential for future improvement. For example, it could be possible to expand the simulation's scope by increasing the nµmber of simulated cardiomyocytes and transitioning from a 2D grid to a full 3D tissue model. Here, we could incorporate spatial organization, cellular heterogeneity, and realistic cell-to-cell interactions within the tissue environment. This extension will enable a more accurate representation of scar formation and progression in a physiologically relevant context. This laser ablation model could also be used to investigate the role of rescue mechanisms during LON (loss of neighbor) events in the context of scar progression. The involvement of fibroblasts and macrophages and their potential rescue mechanisms can be explored within the simulation model. Interactions between cardiomyocytes, fibroblasts, and macrophages can also be incorporated to simulate the dynamic cellular crosstalk involved in scar formation and resolution. Although our model has already shown promise in studying the loss of neighbor theory in myocardial infarction, the possible growth is also something to account for.

3.3. Quantitative Phase Imaging (QPI) Study

Through usage of Quantitative Phase Imaging (QPI), a significant increase in the thickness of the collagen tissue surrounding the laser ablation site, with an observed 30% increase in thickness, from 7.78 to 10.68 µm. Note that although the system can measure the thickness of the collagen tissue, it was unable to take detailed thickness measurements, such as the thin line after the laser ablation which measured 1.12 µm in width. Future studies using this meta-device will focus on the improvement of resolution, so that images may be able to accurately measure to 1 µm or smaller. This novel application of the meta-device QPI technique to collagen tissue represents a significant expansion of the technology's utility in biomedical research and paves the way for future research in other biological tissues using the Eagle-Eye Inspired Meta-Device. The specificity of the imaging results demonstrates the system's versatility and effectiveness in measuring structural changes in different types of biological tissues.

In HEK293 cells, laser ablation caused a noticeable increase in cell thickness in areas surrounding the ablation region, suggesting a movement of cell mass within the cell. The phase imaging process allowed real-time visualization of these changes, something that may be important to future applications such as surgery(Figure 5).

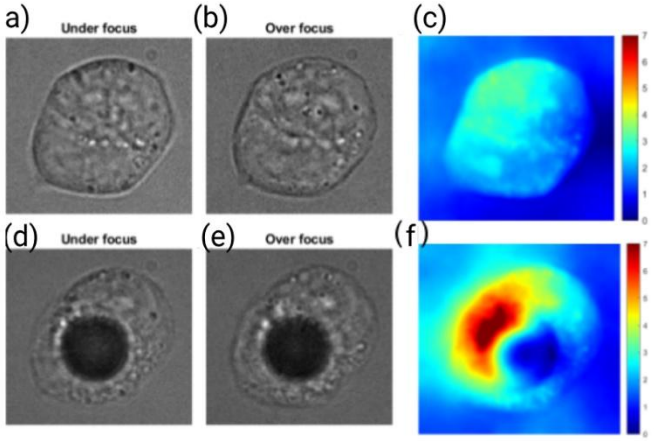

Figure 5. Phase images of HEK293 cells. (a) and (b) are the underfocused and overfocused images after light passes through the meta-device for the cell before ablation. (d) and (e) are after ablation. (c) Image of the cell with thickness indicator before ablation with (f) being after laser ablation for the HEK cell.

With PC-12, we tried a different experimental process, using different power levels and observing their correlated changes. Cell thickness was minimally impacted at the lowest power, 244 mW, with only a 0.50% change observed, shown in Figure 7A. This suggests that the laser energy was insufficient at this power level to induce significant structural alterations in the cells, likely because the energy absorbed was below the threshold needed to cause noticeable expansion through the ablation. At a laser power of 281mW, a substantial increase in cell thickness was observed, with a 77.55% expansion occurring immediately after laser ablation, shown in Figure 7B. This change indicates that the laser power at this level was sufficient to induce damage, increasing cell volµme, likely due to thermal effects or the generation of intracellular stress and swelling. The most pronounced effect was observed at the highest power, 311mW, where the cell thickness increased by 230.53% following laser ablation, shown in Figure 7C. This increase suggests a high degree of cellular disruption, potentially due to the formation of cavitation bubbles or other damage mechanisms induced by the higher energy input. The results imply that as the laser power increases, the extent of cellular damage and subsequent expansion becomes more significant.

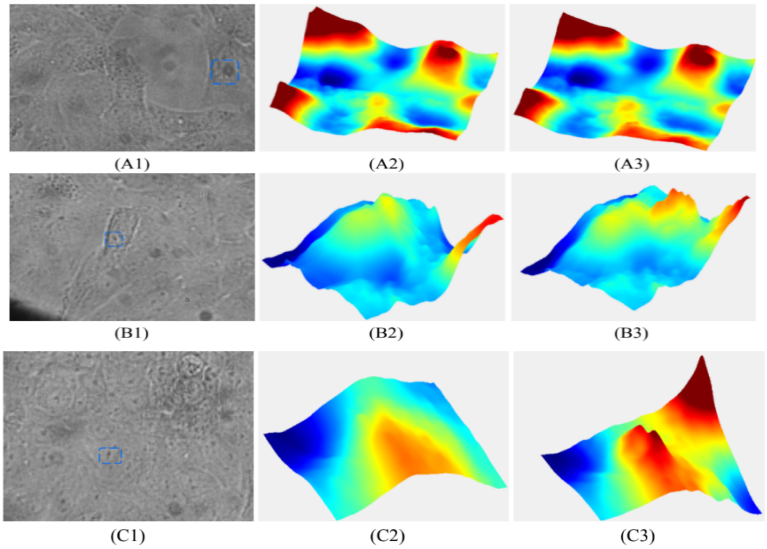

Figure 7. (A) 244 mW at focal plane was applied on the cell in the blue rectangle, (A1) Phase image, (A2) Thickness before laser ablation, (A3) Thickness right after laser ablation. (B) 281 mW at focal plane was applied, (B1) Phase image, (B2) Thickness before laser ablation, (B3) Thickness right after laser ablation. (C) 312 mW at focal plane was applied, (C1) Phase image, (C2) Thickness before laser ablation, (C3) Thickness right after laser ablation.

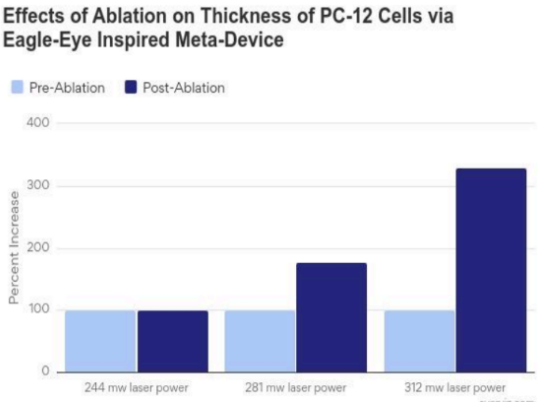

Figure 8. Thickness Change measured in correspondence to laser power, pre- and post-ablation.

Once again, these findings with PC-12 and HEK293 are crucial for understanding the effects of laser ablation on cellular structures. They inform future studies to optimize laser parameters for applications in cellular manipulation, laser surgery, and other biomedical fields.

4. Conclusion

Our study used laser ablation to observe the degeneration of several cell and tissue types, cardiomyocytes, Cortical Neuron cells, collagen fibers, PC12, and HEK293 cells. We aim to introduce laser ablation as a novel and efficient research method to study their reactions to cellular stress, as well as any of their associated degenerative diseases. Utilizing laser ablation on Cortical Neurons, we observed more shrinkage in high-glucose neurons than in low-glucose neurons but were unable to ascertain the significance of this shrinkage. However, our study does demonstrate the potential of laser ablation in measuring the strength of neurons in conditions such as diabetic neuropathy. In the case of Heart Cell death, we were able to use laser ablation to measure changes in border cells from physical stressors. In combination with Quantitative Phase Imaging (QPI), we demonstrated real-time visualization of cell-thickness change. In the future, laser parameters can be further optimized for applications in cellular manipulation, laser surgery, and other biomedical fields. Research could then also explore the underlying mechanisms driving these thickness changes and examine the long-term effects of laser exposure on cell viability and function.

Acknowledgements

We would like to thank Dr. Kevin King's lab for providing the heart. This material was based upon work supported by a gift from Beckman Laser Institute Inc. to L.S. and V.G.G.. Special thanks to the private donors to our UCSD IEM BTC center: Dr. Shu Chien from UCSD Bioengineering, Dr. Lizhu Chen from CorDx Inc., Dr. Xinhua Zheng, David & Leslie Lee for their generous donations.

References

[1] M. W. Berns, "Laser Scissors and Tweezers," *Frontiers of Bioengineering and Biotechnology*, vol. 278, no. 4, pp. 62–67, Apr. 1998, doi: https://doi.org/10.1038/scientificamerican0498-62.

[2] L. Jia, L. Wang, M. Chopp, Y. Zhang, A. Szalad, and Z. G. Zhang, "MicroRNA 146a Locally Mediates Distal Axonal Growth of Dorsal Root Ganglia Neurons under High Glucose and Sildenafil Conditions," *Neuroscience*, vol. 329, pp. 43–53, Aug. 2016, doi: https://doi.org/10.1016/j.neuroscience.2016.05.005.

[3] M. Saleh and J. A. Ambrose, "Understanding Myocardial Infarction," *F1000Research*, vol. 7, no. 1, p. 1378, Sep. 2018, doi: https://doi.org/10.12688/f1000research.15096.1.

[4] K. R. King, D. M. Calcagno, N. Taghdiri, A. Toomu, V. Ninh, and Z. Fu, “SINGLE CELL AND SPATIAL TRANSCRIPTOMICS OF THE ISCHEMIC BORDERZONE,” *Journal of the American College of Cardiology*, vol. 79, no. 9, Apr. 2022, doi: https://doi.org/10.1016/S0735-1097(22)01962-3.
[5] N. Yu, P. Genevet, M. Kats, F. Aieta, J. P. Tentienne, F. Capasso, and Z. Gaburro, “Light Propagation with Phase Discontinuities: Generalized Laws of Reflection and Refraction,” *Science*, vol. 334, no. 6054, pp. 333–337, Sep. 2011, doi: https://doi.org/10.1126/science.1210713.
[6] J. Zhou and Z. Liu, “Photonic spin-dependent wave shaping with metasurfaces: applications in edge detection,” *Plasmonic Materials and Metastructures*, pp. 227–243, Sep. 2023, doi: https://doi.org/10.1016/b978-0-323-85379-8.00008-3.
[7] T. J. Cui, S. Zhang, A. Alù, M. Wegener, J. Pendry, J. Luo, Y. Lai, Z. Wang, X. Lin, and H. Chen, “Roadmap on electromagnetic metamaterials and metasurfaces,” *Journal of Physics: Photonics*, vol. 6, no. 3, p. 032502, Jul. 2024, doi: https://doi.org/10.1088/2515-7647/ad1a3b.
[8] W. Yang, J. Zhou, D. P. Tsai, and S. Xiao, “Advanced manufacturing of dielectric meta-devices,” *Photonics Insights*, vol. 3, no. 2, p. R04, 2024, doi: https://doi.org/10.3788/pi.2024.r04.
[9] J. Zhou, Q. Wu, J. Zhao, C. Posner, M. Lei, G. Chen, J. Zhang, and Z. Liu, “Fourier Optical Spin Splitting Microscopy,” *Physical Review Letters*, vol. 129, no. 2, Jul. 2022, doi: https://doi.org/10.1103/physrevlett.129.020801.
[10] J. Zhou, F. Tian, J. Hu, L. Z. Shi, V. G. Godinez, D. P. Tsai, and Z. Liu, “Eagle-Eye Inspired Meta-Device for Phase Imaging,” *Advanced Materials*, vol. 36, no. 32, p. 202402751, Jun. 2024, doi: https://doi.org/10.1002/adma.202402751.
[11] Q. Wu, J. Zhou, X. Chen, J. Zhao, M. Lei, G. Chen, Y. Lo, and Z. Liu, “Single-shot quantitative amplitude and phase imaging based on a pair of all-dielectric metasurfaces,” *Optica*, vol. 10, no. 5, p. 619, May 2023, doi: https://doi.org/10.1364/optica.483366.
[12] P. Wang, J. Liang, L. Z. Shi, Y. Wang, P. Zhang, M. Ouyang, D. Preece, Q. Peng, L. Shao, J. Fan, J. Sun, S. S. Li, M. W. Berns, H. Zhao, and Y. Wang, “Visualizing Spatiotemporal Dynamics of Intercellular Mechanotransmission upon Wounding,” *ACS photonics*, vol. 5, no. 9, pp. 3565–3574, Aug. 2018, doi: https://doi.org/10.1021/acsphotonics.8b00383.
[13] L. G. W. Hilgenberg and M. A. Smith, “Preparation of Dissociated Mouse Cortical Neuron Cultures,” *Journal of Visualized Experiments*, vol. 562, no. 10, Dec. 2007, doi: https://doi.org/10.3791/562.
[14] “Neonatal Cardiomyocyte Isolation System - Manual.,” *www.worthington-biochem.com*. https://www.worthington-biochem.com/products/neonatal-cardiomyocyte-isolation-system/manual (accessed Feb. 22, 2024).
[15] “Bovine Collagen, Type I Polymeric (Insoluble).” Accessed: Dec. 03, 2024. [Online]. Available: https://advancedbiomatrix.com/public/pdf/Collagen/5162-DFU-Bovine-Collagen-type-I-Lyophilized-Fibrous-Powder-1-gram-Rev-05.pdf
[16] J. Zhou, H. Qian, H. Luo, S. Wen, and Z. Liu, “A spin controlled wavefront shaping metasurface with low dispersion in visible frequencies,” *Nanoscale*, vol. 11, no. 36, pp. 17111–17119, 2019, doi: https://doi.org/10.1039/c9nr03566d.
[17] J. Zhou, H. Qian, G. Hu, H. Luo, S. Wen, and Z. Liu, “Broadband Photonic Spin Hall Meta-Lens,” *ACS Nano*, vol. 12, no. 1, pp. 82–88, Dec. 2017, doi: https://doi.org/10.1021/acsnano.7b07379.
[18] J. Zhang, Q. Chen, J. Sun, L. Tian, and C. Zuo, “On a universal solution to the transport-of-intensity equation,” *Optics Letters*, vol. 45, no. 13, pp. 3649–3652, Jul. 2020, doi: https://doi.org/10.1364/OL.391823.